Mon. Not. R. astr. Soc. (1985) **217**, 367–386

Hydrodynamic calculations of axisymmetric accretion flow

Eiji Shima,★ Takuya Matsuda, Hidenori Takeda and Keisuke Sawada★ *Department of Aeronautical Engineering, Kyoto University, Kyoto 606, Japan*

Accepted 1985 June 20. Received 1985 June 11; in original form 1985 April 10

Summary. Numerical calculations are performed for axisymmetric flow of inviscid ideal gas past a gravitating body. Cases based on two extreme boundary conditions on the surface of the body, i.e. a slippery condition on a rigid sphere and a maximum accretion condition on a hollow sphere, are computed and compared. The results are presented for Mach numbers of 0.6, 1.4, 2.4 and 5.0, and for the ratio of specific heats of 1.1, 4/3 and 5/3.

Supersonic flow passing an absorbing object shows a shock cone, which is a detached bow shock in the case of $\gamma=5/3$ while it is attached to the surface of the hollow sphere in the case of $\gamma=1.1$. The density is significantly higher immediately behind the shock than along the accretion axis in the cases of $\gamma=5/3$ and 4/3, and therefore it is appropriate to call it an accretion cone rather than an accretion column. However, in the case of $\gamma=1.1$, an accretion column is formed.

Global features of the flow past a gravitating rigid sphere are similar to those of the accreting case except very close to the body, where a counter current is formed.

An accretion rate and a drag coefficient are computed and compared with the theoretical estimates, and reasonable agreements between them are obtained.

1 Introduction

The gravitational interaction between an astronomical object and surrounding gas has been the subject of many astrophysical studies. Typical examples are the motion of a galaxy through an intracluster gas, the collision of a star with an interstellar cloud, and the interaction of a compact object with the stellar wind of a giant companion in a close binary system.

A lot of works have been performed to compute the accretion flow about various objects. However, it is essential to clarify the hydrodynamic aspects of the accretion flow before applying the calculations to realistic problems. The inclusion of complicated physical processes such as cooling, heating, radiative transfer, turbulence and realistic gravitational potential, etc. may

★Aircraft Engineering Division, Kawasaki Heavy Industries Ltd, Kakamigahara, Gifu-Pref. 504, Japan.

obscure the results. The aim of the present work is to supply the flow patterns, the accretion rate and the drag by computing the axisymmetric accretion flow under simplified conditions. The computations are performed on the frame of the gravitating object.

Let us view the history of the accretion theory. If the gas is assumed to be sufficiently rarefied, particle collisions and pressure can be neglected except along the downstream axis. Close to this accretion axis particle collisions would become important. These collisions destroy the transverse momentum but leave its radial momentum unchanged. If the resultant velocity of the particle at the axis is less than the escape velocity, it will be captured by the body.

In such a case an accretion rate, A, is given by Hoyle & Lyttleton (1939) as

$$A=\pi R_{\mathrm{A}}^2\varrho_\infty V=4\pi(GM)^2\varrho_\infty/V^3, \tag{1.1}$$

where ϱ_∞ and V are the density and the velocity of the upstream gas, respectively, and R_{A} is the 'accretion radius' defined by

$$R_{\mathrm{A}}=2GM/V^2. \tag{1.2}$$

Here G is the gravitational constant and M is the mass of the object.

Bondi & Hoyle (1944) introduced a parameter α into the accretion rate in order to avoid the infinite density along the accretion axis. They introduced a notion of an 'accretion column' which is a column of gas of finite density. They had

$$A=\alpha\pi R_{\mathrm{A}}^2\varrho_\infty V. \tag{1.3}$$

According to them, the value of α lies in the range $\frac{1}{2}<\alpha<1$. These formula are applicable for highly supersonic flows.

A case of spherically symmetric accretion was first considered by Bondi (1952), who introduced a characteristic length corresponding to the accretion radius called the 'Bondi radius' given by

$$R_{\mathrm{B}}=GM/c_\infty^2, \tag{1.4}$$

where c_∞ is the sound speed at infinity. The accretion rate is given by

$$A=4\pi\lambda R_{\mathrm{B}}^2\varrho_\infty c_\infty=4\pi\lambda(GM)^2\varrho_\infty/c_\infty^3, \tag{1.5}$$

where λ is a non-dimensional parameter of order unity depending on the specific heat ratio γ. These two expressions (1.3) and (1.5) are valid at the extremes $M_\infty\gg1$ and $M_\infty=0$ respectively, where M_∞ is the Mach number of the flow at large distances. Bondi (1952) suggested an interpolation formula for an intermediate case:

$$A\sim2\pi(GM)^2\varrho_\infty/(c_\infty^2+V^2)^{3/2}. \tag{1.6}$$

However, other interpolation formulae are possible as well.

In the derivation of equations (1.1) to (1.3), we have regarded particles as non-interacting except in the accretion column. However, in many cases the mean free path of gas will be much smaller than the accretion radius and the radius of the body. Therefore it is necessary to treat the process hydrodynamically.

In spite of this, the pressure is negligible in a highly supersonic flow, thus the streamline will be given by free particle orbits except in the accretion column bounded by a shock. Considering these, it would be possible to construct a semi-analytic solution.

Ruderman & Spiegel (1971) assumed a trailing shock originating behind the body and obtained simplified numerical solutions. As will be seen later, however, such a configuration is not realized in our fully numerical calculations.

Wolfson (1977) sought a self-similar solution assuming R_{A} to be infinitely large and the shock front to be conical. His work was extended by Bisnovatyi-Kogan *et al.* (1979). They concluded

that a self-similar solution exists only when $1.31<\gamma<5/3$. A solution with a hollow space behind the gravitating body exists as well. In their solutions density becomes infinite on the symmetry axis or the surface of the hollow cone. It is interesting to know if their flow patterns are realized in our hydrodynamic calculations.

Numerical study of intermediate cases was first performed by Hunt (1971) using the Lax–Wendroff method. A flow for $M_\infty=0.6$, 1.4 and 2.4 with $\gamma=5/3$ was calculated, and the interpolation formula (1.6) was confirmed. Hunt assumed vanishing pressure and density on the surface of the accreting object; thus his inner boundary condition was equivalent to that of maximum accretion rate. It was reported that a supersonic flow possessed a bow shock similar to that given by a blunt-nosed object in a supersonic air flow in spite of the absorbing boundary condition. He also computed the case of $\gamma=4/3$ and obtained similar results (Hunt 1979).

On the other hand, an adiabatic flow past a rigid gravitating sphere was calculated by Shara & Shaviv (1980), also using the Lax–Wendroff method. Livio, Shara & Shaviv (1979) applied their method of calculation to a model for a compact X-ray source. Their flow patterns were essentially the same as these of Shara & Shaviv, but very different from these of Hunt. They insisted that the shape of shock was not conical but closed around a gravitating body. They ascribe the discrepancy mainly to the difference in the boundary condition.

Recently Takeda *et al.* (1985) computed a viscous flow past a gravitating solid sphere in order to estimate the drag coefficient using an implicit Beam–Warming scheme. The range of their Mach number was from 0.5 to 2. They obtained similar flow patterns to Hunt (1971) rather than to Shara & Shaviv (1979). One of the objectives of the present work is to clarify which type of flow is more realistic for supersonic inviscid flows.

There are some difficulties in the calculation of a flow affected by gravity. Even if the Mach number at infinity is small, a fluid is accelerated by gravitational attraction and a very strong shock wave is produced near a gravitating body. Ordinary centred difference schemes such as the Lax–Wendroff scheme and the Beam–Warming scheme are not robust enough to simulate a very strong shock wave. In order to calculate the flow stably, it is normal to use an artificial viscosity and/or filter. However, in order to stabilize a strong shock wave, excessive numerical viscosity is often introduced. It smooths off the shock wave and causes gross errors in other region of the flow.

Hunt avoided this difficulty by determining the position of the shock wave by 'shock fitting', in which the variables behind the shock wave were calculated by the Rankine–Hugoniot shock conditions. He also assumed that the density and the entropy were not less than those at infinite upstream. Although his method seems to be very smart, it would be difficult to apply to more complex situations.

We try to solve this problem by using a modern technique of Computational Fluid Dynamics, fine meshes and a fast super computer. In our calculations, the finite volume version of second-order accurate Osher scheme is applied (see Chakravarthy & Osher 1983 for the finite-difference version of the first-order accurate Osher scheme).

The Osher scheme is an upwind, shock-capturing algorithm for hyperbolic equations, and does not need artificial viscosity to stabilize the solution. It is based on a Riemann problem solver, as is Godunov's (1959) scheme, but shocks are approximated by compression waves. Since Osher scheme does not need iterations to find the solution to the Riemann problem; it is much more efficient to implement in a vector computer.

The Godunov type schemes generally do not show wiggles near shocks or contact surfaces, which are sometimes fatal to the computation. They are more robust than ordinary centred difference schemes. The shock waves contain only one to two transition points.

In order to test the present scheme, a flow around a non-gravitating rigid sphere in the air is calculated. Results are compared with experiments, and a good agreement is obtained. Next,

we compute the accretion flow on to a body permitting maximum accretion and a flow about a non-accreting gravitating solid spherical body.

In accreting case, a flow for upstream Mach number 0.6, 1.4, 2.4 and 5.0 with specific heat ratio $\gamma=1.1$, 4/3 and 5/3 is calculated, and the accretion rate and drag are obtained. In non-accreting case, a flow for upstream Mach number 0.6, 1.4, 2.4, 5.0 with $\gamma=5/3$ is calculated and the drag is computed.

2 Formulation

2.1 BASIC EQUATIONS

In our calculations we neglect the viscosity and thermal conductivity. The equation describing a perfect gas including the gravitational force is written in the form of

$$\mathbf{Q}_t+\mathbf{E}_x+\mathbf{F}_y+\mathbf{G}_z+\mathbf{S}=0, \tag{2.1}$$

where

$$\mathbf{Q}=\begin{pmatrix}\varrho\\ \varrho u\\ \varrho v\\ \varrho w\\ e\end{pmatrix},\quad \mathbf{E}=\begin{pmatrix}\varrho u\\ \varrho u^2+p\\ \varrho uv\\ \varrho uw\\ (e+p)u\end{pmatrix},\quad \mathbf{F}=\begin{pmatrix}\varrho v\\ \varrho uy\\ \varrho v^2+p\\ \varrho vw\\ (e+p)v\end{pmatrix},\quad \mathbf{G}=\begin{pmatrix}\varrho w\\ \varrho uw\\ \varrho vw\\ \varrho w^2+p\\ (e+p)w\end{pmatrix},$$

$$\mathbf{S}=\begin{pmatrix}0\\ GM\varrho x/r^3\\ GM\varrho y/r^3\\ GM\varrho z/r^3\\ GM\varrho(xu+yv+zw)/r^3\end{pmatrix}. \tag{2.2}$$

Here ϱ is the density, u, v and w are the velocity components in the Cartesian coordinate, p is the pressure, $r=(x^2+y^2+z^2)^{1/2}$ is the distance from the gravitational centre, and e is the energy per unit volume given by

$$e=p/(\gamma-1)+\varrho(u^2+v^2+w^2)/2, \tag{2.3}$$

where γ is the specific heat ratio.

We solve the time-dependent equations numerically in an axisymmetric coordinate system until steady states are reached.

2.2 FINITE-VOLUME DISCRETIZATION

In the present work we use a finite-volume version of Osher scheme with the second order of accuracy. As to the finite-difference version of Osher scheme with the first order of accuracy, see Chakravarthy & Osher (1983) and Osher & Chakravarthy (1983). The technique to make the method second-order accurate is due to van Albada, van Leer & Roberts (1982). The detail of the computational method is to be published elsewhere and is available from the authors.

The Euler equations (2.1) can be written in integral form for a fixed region Ω with boundary $\partial\Omega$ as

$$\int_\Omega \mathbf{Q}_t\, dV+\int_{\partial\Omega}(n_1\mathbf{E}+n_2\mathbf{F}+n_3\mathbf{G})\, ds+\int_\Omega \mathbf{S}\, dV=0 \tag{2.4}$$

where (n_1, n_2, n_3) is a unit outward vector normal to the boundary wall, and the flux **E**, **F** and **G** and the source term **S** are given in (2.2). Equation (2.4) is applied for a discretized computational cell and is approximated using the finite-volume discretization (Jameson & Baker 1983; Rizzi 1982). The flux between two cells is given by the solution of the Riemann problem. It is solved approximately using the Osher scheme.

We assume axisymmetry and that an azimuthal velocity vanishes. A special treatment for the axial singularity is needless in the present scheme, since the area of the boundary interface at the axis merely vanishes and the flux is taken to be zero there.

2.3 THE COMPUTATIONAL REGION, THE INITIAL CONDITIONS AND THE BOUNDARY CONDITIONS

The region of calculation used in the present work is a spherical region truncated by a central sphere. We denote the radius of the central body (or the central hollow hole) by $r_{\min}$ and radius of the outer boundary to be $r_{\max}$. Following Ruderman & Spiegel (1971), we introduce a non-dimensional parameter δ as

$$\delta=R_A/r_{\min}. \tag{2.7}$$

We fix δ to be 10 throughout our calculations.

The number of meshes is 50 in the radial direction and 30 in the tangential direction. The number of mesh points used by Hunt (1971) is 36×12 although his $r_{\max}/r_{\min}$ is 10^4. In our case this value is 116. Shara & Shaviv's (1979) mesh is 44×18. Therefore our mesh is much finer than those of the above authors.

The computations are started from the initial condition of the uniform flow in which all variables in the region are taken to be those at infinity. Beyond the outer boundary we assume there is undisturbed gas moving with constant Mach speed M_∞. The values at the outer boundary are computed by solving the Riemann problem, and therefore rigorous boundary conditions can be applied.

In our calculations, we consider two types of inner boundary conditions. For the accreting case,

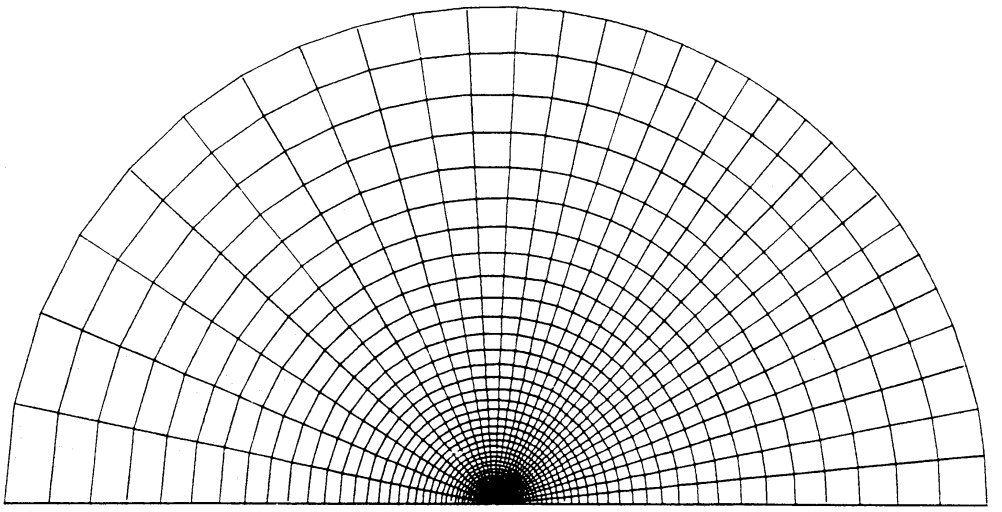

Figure 1. The computational grid system.

density and pressure are taken to be zero as in the calculation of Hunt (1971). Therefore the central body is a hollow sphere. The boundary condition then gives the maximum accretion rate for the case of spherically symmetric accretion.

For the flow about a non-accreting rigid sphere, we adopt the slippery boundary condition in which the radial velocity vanishes and the tangential velocity is not affected on the surface.

The computations were performed mainly by the Fujitsu VP100 vector processor. Its maximum speed was announced to be 260 MFLOPS, which should be compared with 10 MFLOPS for the Fujitsu M380 scalar computer. Since our numerical code has long DO loops containing complex switches, we could achieve only 70 to 80 MFLOPS. One case takes 7–15 min.

3 Results

3.1 FLOW ABOUT A NON-GRAVITATING RIGID SPHERE

In order to examine the accuracy and the robustness of the scheme, flows in the air ($\gamma=1.4$) for various Mach number, i.e. $M_\infty=0.5$, 0.8, 1.53, 4.01 and 7.6, are calculated. They are compared

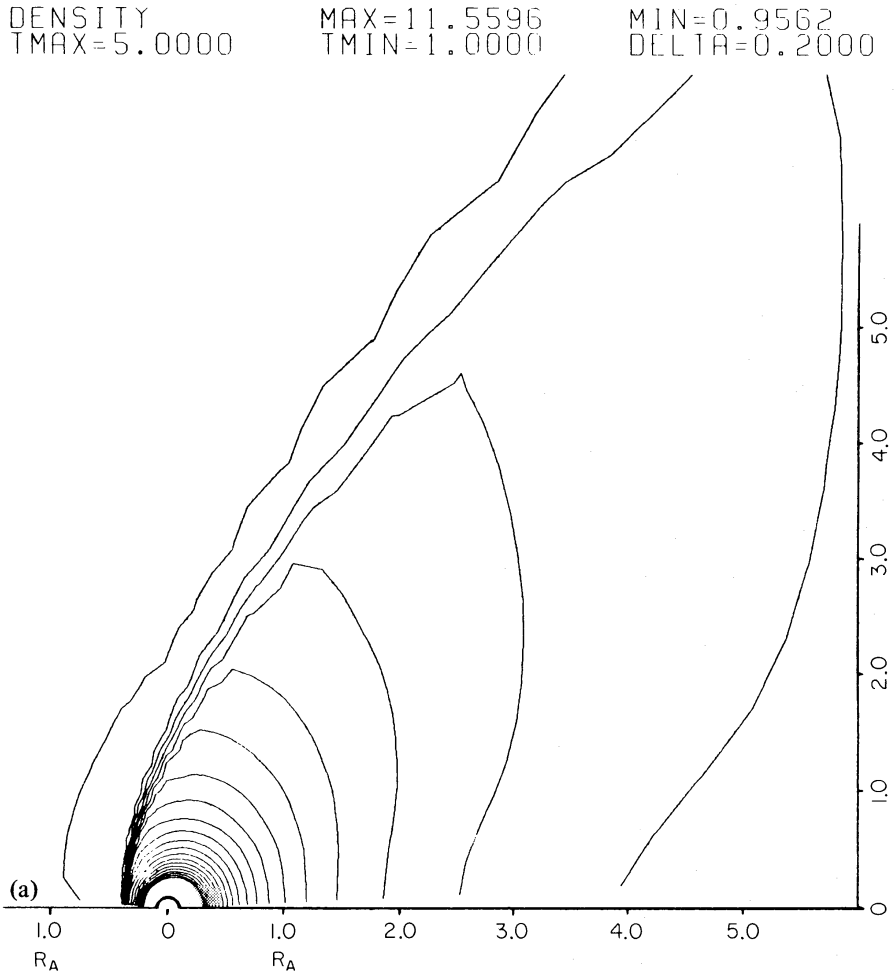

Figure 2. (a) Density contours for the accretion flow with the Mach number 1.4 and the specific heat ratio 5/3. Lengths are scale by the accretion radius R_A. R_A on the horizontal axis shows the position of accretion radius. The maximum and the minimum of the non-dimensional density in the region are 11.5596 and 0.9562, respectively. In the figure the density contours between 1–5 is shown with the same increment, 0.2. Since the physical quantities are defined at the cell centre, those at the symmetry axis are not given. (b) Close-up look of the Mach number contours and the velocity vectors for the same model as Fig. 2a. The thick line shows the sonic line on which the local Mach number is unity. Note that the stagnation point occurs at about $0.4R_A$ on the rear axis. (c) Entropy contours and the velocity vectors for the same model as Fig. 2a. As long as the flow is steady and numerical error is absent, isentropic lines coincide with the streamlines.

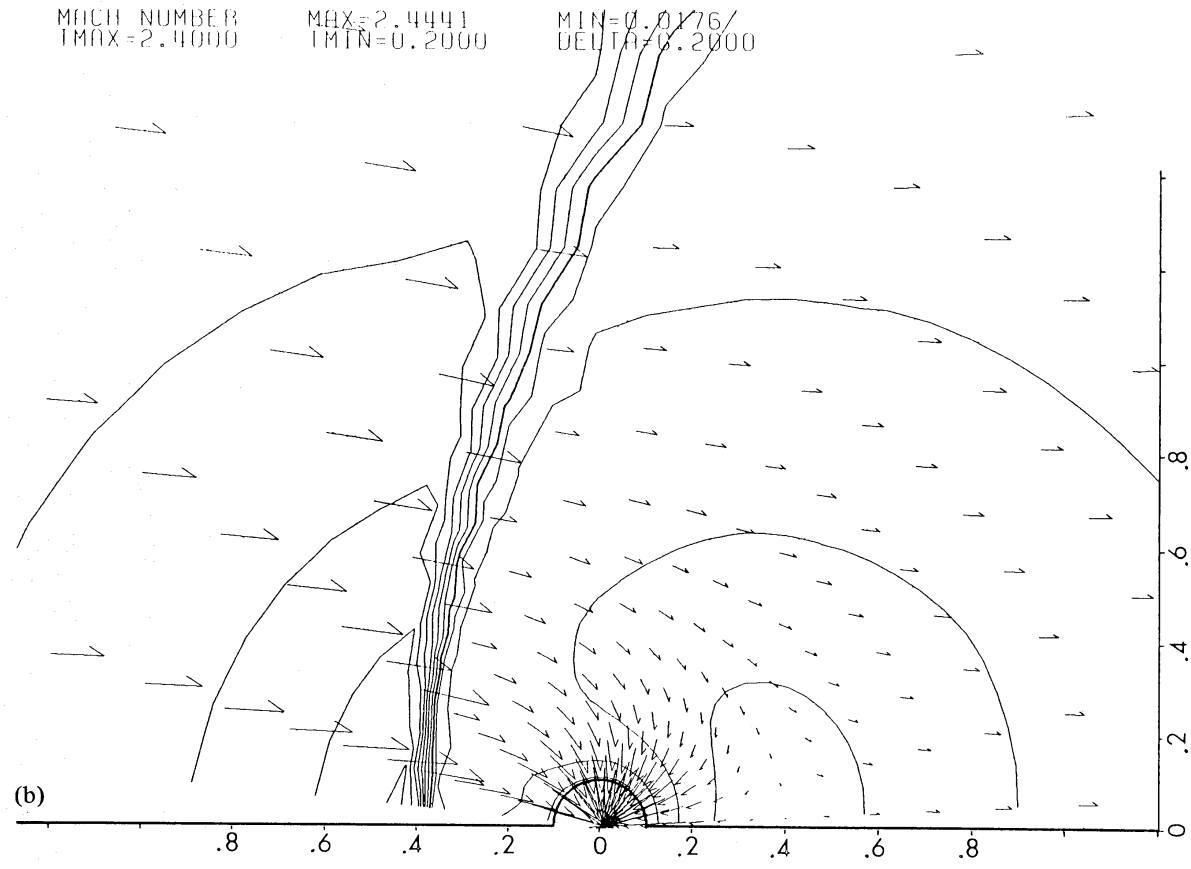

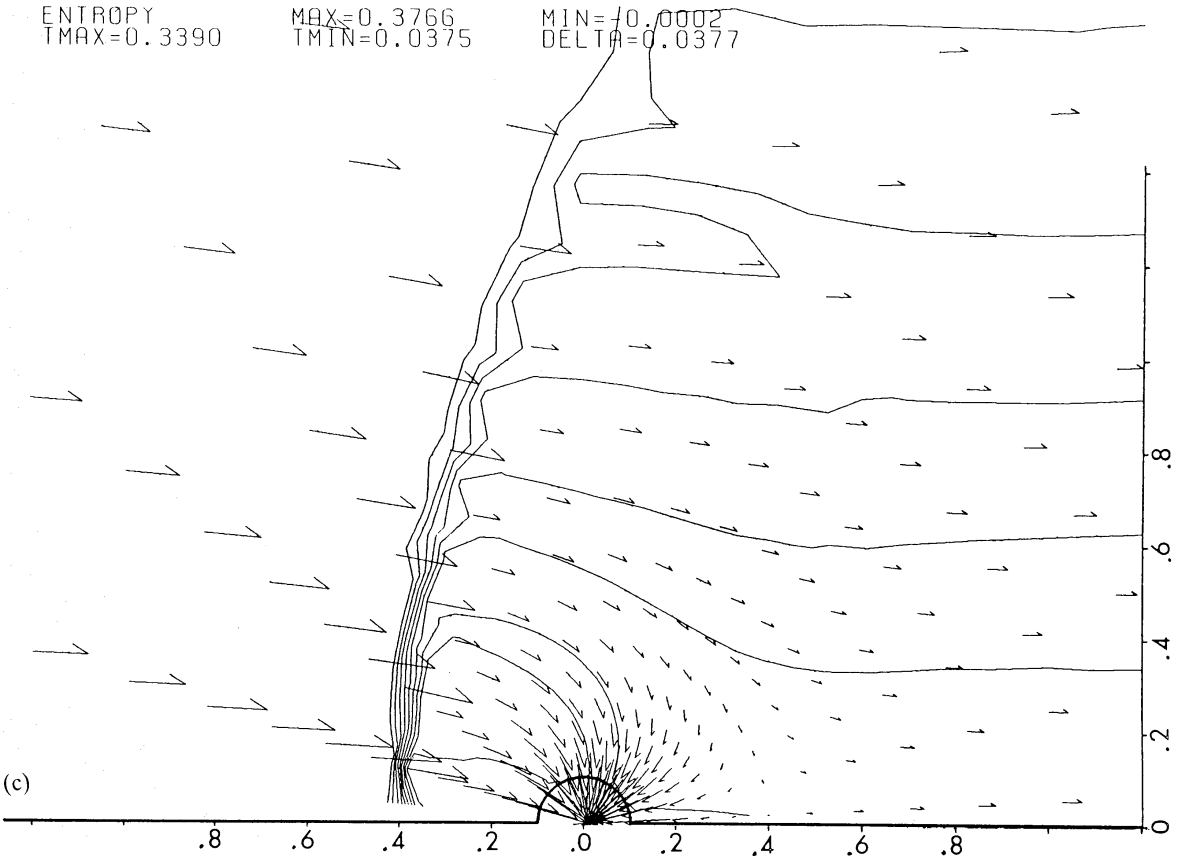

Figure 2 – *continued*

with the shadowgraph of the experiments at the same condition (Van Dyke 1982). The shape and the location of the bow shock wave agree well with those of the experiments.

In the case of hypersonic flow, pressure distribution on the sphere is compared with the theoretical value for a hemisphere computed by the modified Newtonian formula (Lees 1955). Good agreement with the theory is obtained.

The region of a turbulent wake in the experiment is, however, replaced by an eddy behind the body in our results, and the separation of the laminar boundary layer cannot be found. Since the viscosity is neglected and the slippery boundary condition is adopted in our calculations, these disagreements are unavoidable.

3.2 ACCRETION FLOW WITH SPECIFIC HEAT RATIO 5/3 AND VARIOUS MACH NUMBERS

The computational grids used for the gravitating case is shown in Fig. 1. The cases for the Mach number at infinite, M_∞, of 0.6, 1.4, 2.4 and 5.0 with specific heat ratio $\gamma=5/3$ are calculated and compared in this subsection. These calculations have been done for the same Mach number and the same specific heat ratio as Hunt's calculation (1971) except the Mach number 5.0.

The density contours for the subsonic case at Mach speed 0.6 are almost isotropic about the centre. Although the fluid is accelerated by gravitational attraction, the magnitude of the local Mach number is always less than unity and the accretion flow is subsonic.

Three supersonic cases were studied for Mach speeds 1.4, 2.4 and 5.0. All cases possess bow

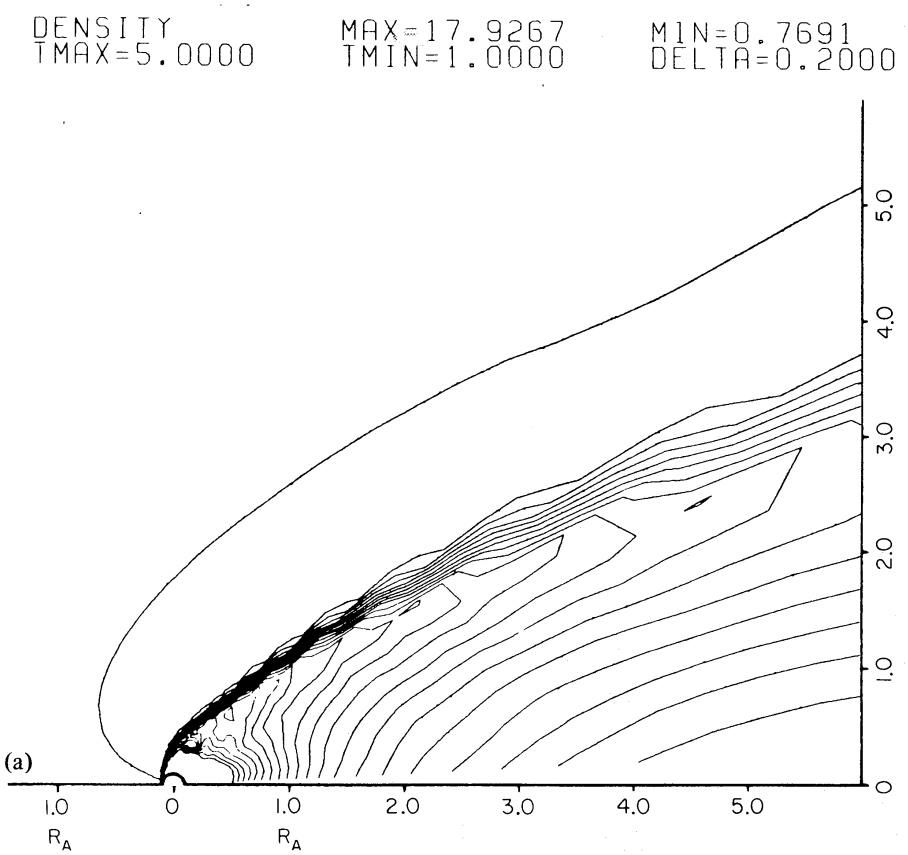

Figure 3. (a) Same as Fig. 2a for Mach number is 5.0. (b) Same as Fig. 2b except for Mach number 5.0. Note that the sonic line begins to depart from the shock line, which indicates that the shock position and the sonic line do not necessarily coincide. Supersonic accretion can be observed behind the sphere. The stagnation point is about R_A, and it validates the estimation of accretion rate due to the line accretion theory. (c) Same as Fig. 2c except for Mach number 5.0.

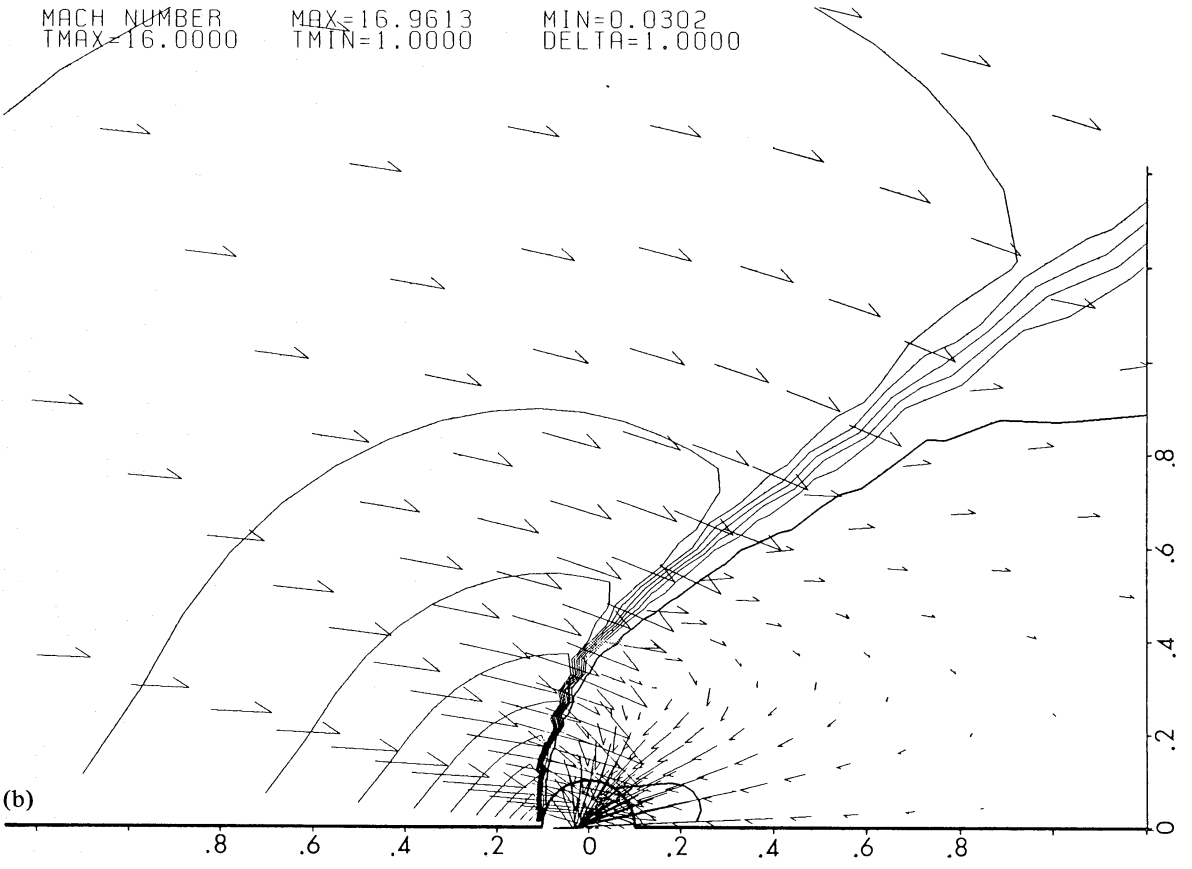

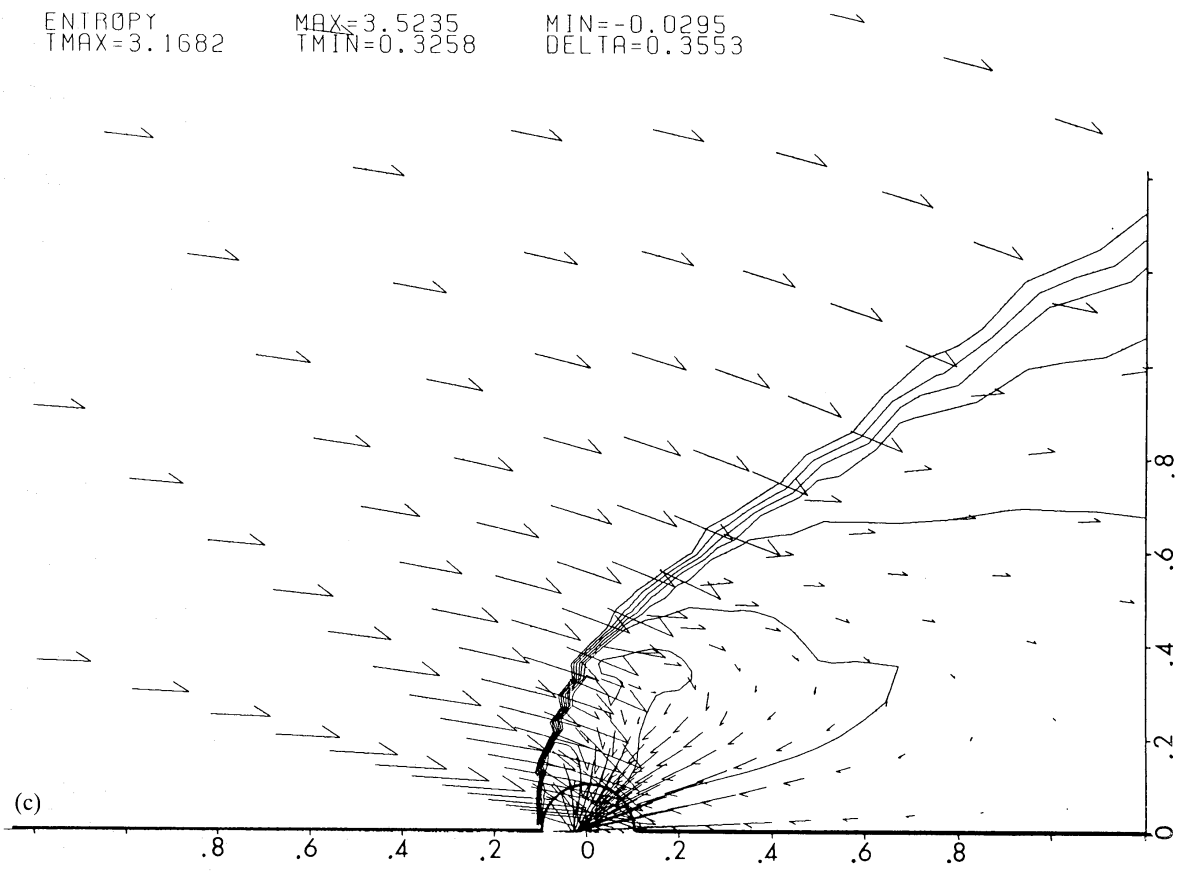

Figure 3 – *continued*

shock waves, as was shown in Hunt's calculations. As gas is drawn gravitationally toward the gravitational source, it becomes denser, and creates pressure forces which support the shock.

Fig. 2a shows the density contours for the flows with the Mach number 1.4. It can be found that the density pattern has ridges just behind the shock cone rather than along the accretion axis. This pattern of density distribution is more evident for the case of $M_\infty = 5.0$, which will be shown in Fig. 3a. Therefore it is appropriate to call the density pattern as an 'accretion cone' rather than an 'accretion column'.

The pressure contours are similar to the density contours about the shock, while they are almost spherical near the axis. Qualitative features of the present calculations agree very well with Hunt's results.

Fig. 2b shows the enlarged view of the Mach number contours as well as the velocity vectors. The thick line shows a sonic line, on which a local Mach number is unity. The sonic line agrees with the shock in this case. Gas accretes on to the hollow sphere subsonically all over the spherical surface.

The stagnation point at which velocity becomes zero appears at about $0.4R_A$ on the rear axis. The gas inside the surface caused by the streamlines hitting the stagnation point is absorbed by the sphere. Therefore the position of the stagnation point is important to determine the accretion rate.

Fig. 2c shows entropy contours, in which entropy is defined as $\log(p/\varrho^\gamma)$. It can be seen that the entropy increases suddenly at the shock front. Behind the shock the isentropic lines should

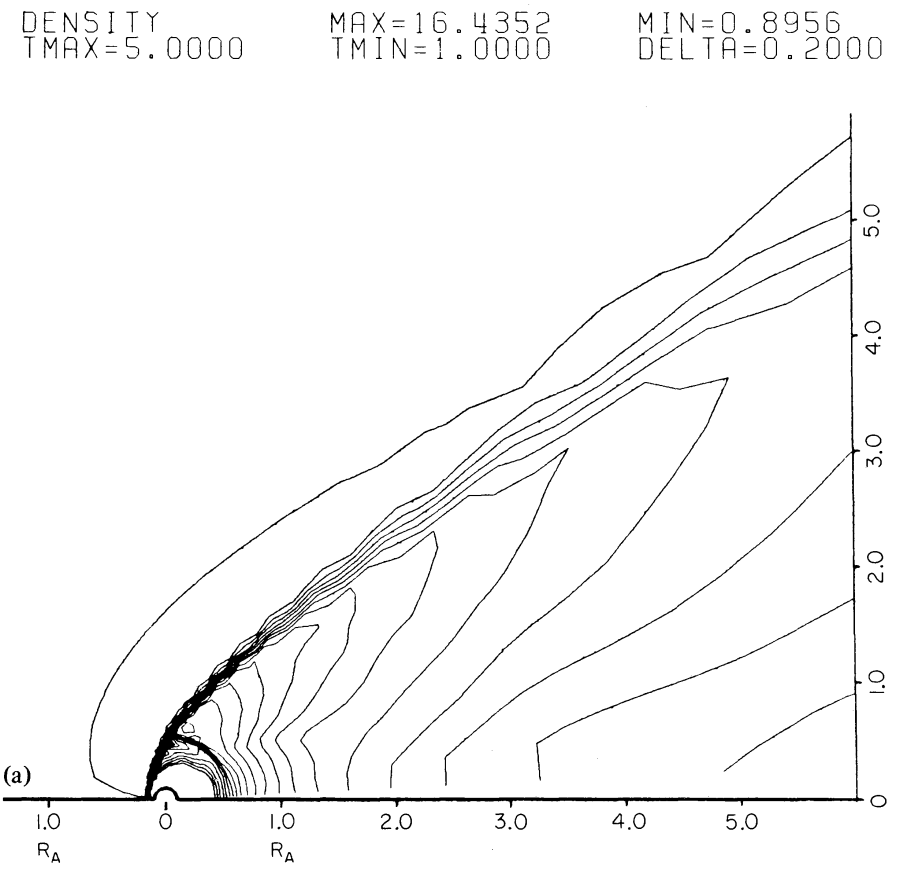

Figure 4. (a) The density contours for the accretion flow with Mach number 2.4 and the specific heat ratio 5/3. (b) Mach number contours and the velocity vectors for the same model as Fig. 4a. (c) Entropy contours for the same model as Fig. 4a.

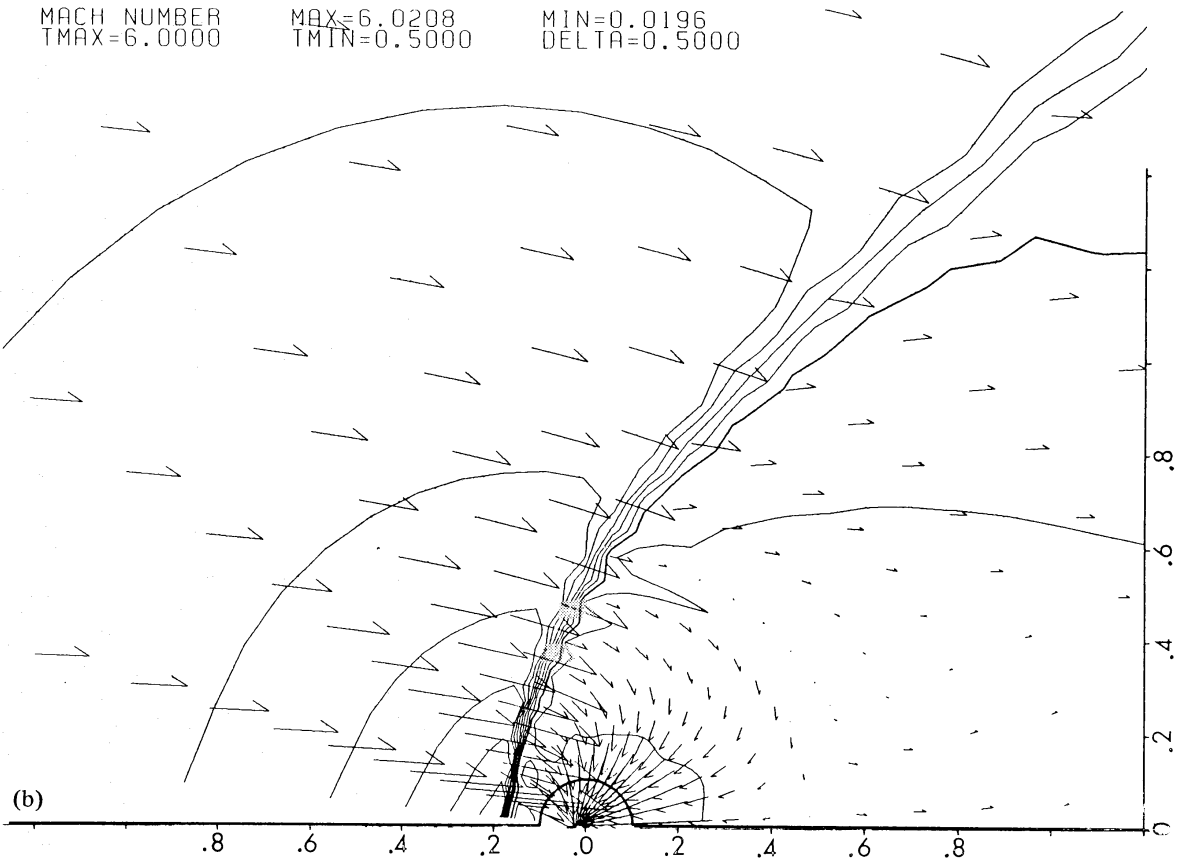

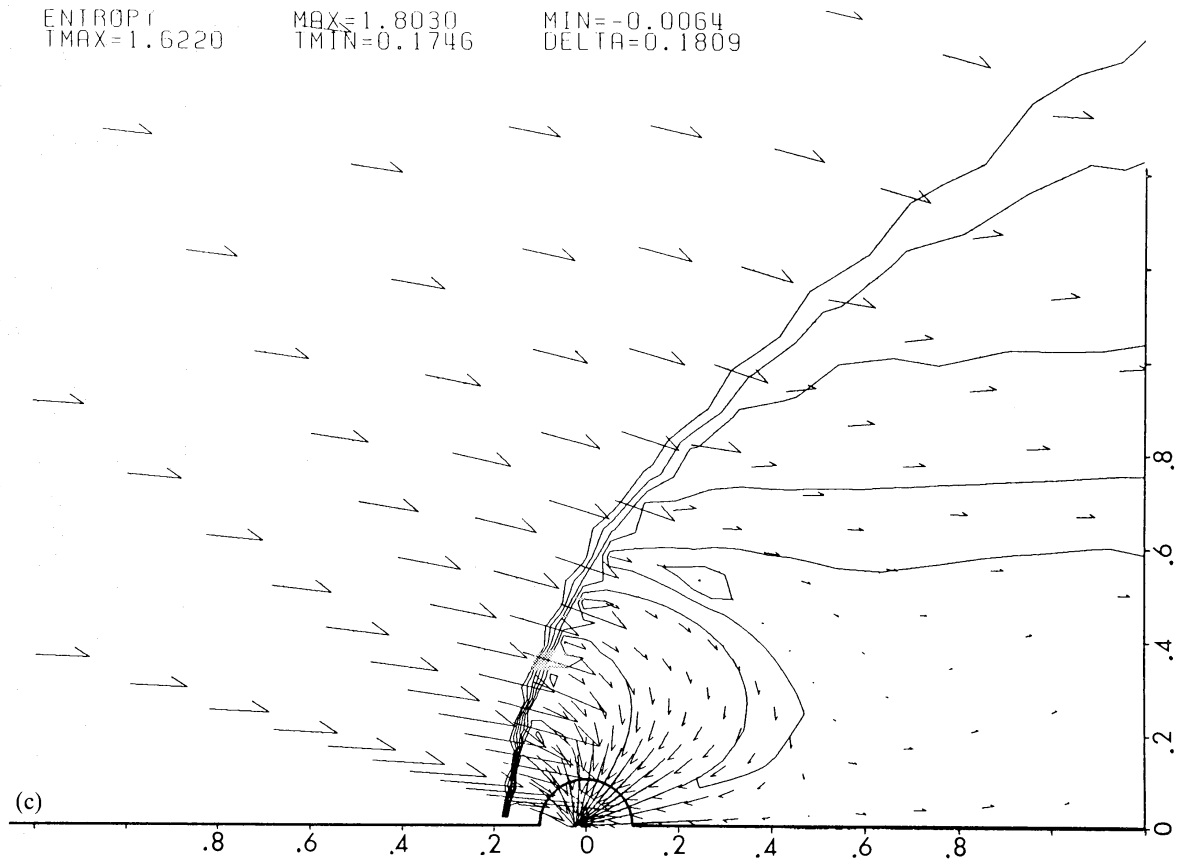

Figure 4 – *continued*

coincide with the streamlines, as long as steady state conditions exist and numerical errors are absent.

Fig. 3a, b and c show the density, the Mach number and the entropy contours, respectively, for the case of $M_\infty=5.0$ and $\gamma=5/3$. As can be seen in Fig. 3a the shock angle is much smaller than the case of $M_\infty=1.4$. Fig. 3b shows that the Mach number just in front of the sphere is as large as 16.96 in this case compared with 2.44 for the case of $M_\infty=1.4$. It should be noted that the sonic line begins to deviate from the shock. This fact tells us that a supersonic–supersonic transition occurs in a strong oblique shock.

It can be seen that the stagnation radius is much larger than in the former case. Since a sonic line appears behind the body, gas accretes supersonically on to the sphere from the rear side.

3.3 DEPENDENCE OF THE FLOW PATTERN ON THE SPECIFIC HEAT RATIO

The accretion flow with specific heat ratios 1.1 and 4/3 are calculated and compared with the case of $\gamma=5/3$. The former is to approximate the isothermal gas ($\gamma=1.0$), and the latter the radiative gas, respectively. In the perfectly isothermal case, the Riemann invariants used in the Osher scheme are quite different from the present case. Therefore we do not give the solution for the perfectly isothermal gas.

In the subsonic cases, the density contours are nearly isotropic as in the case of $\gamma=5/3$. The maximum density, however, becomes larger for smaller specific heat ratio. Although the velocity fields are very similar to those of the flow with $\gamma=5/3$, the magnitude of the local Mach number is greater than unity in front of the inner boundary, which shows that gas accretes supersonically on to a body.

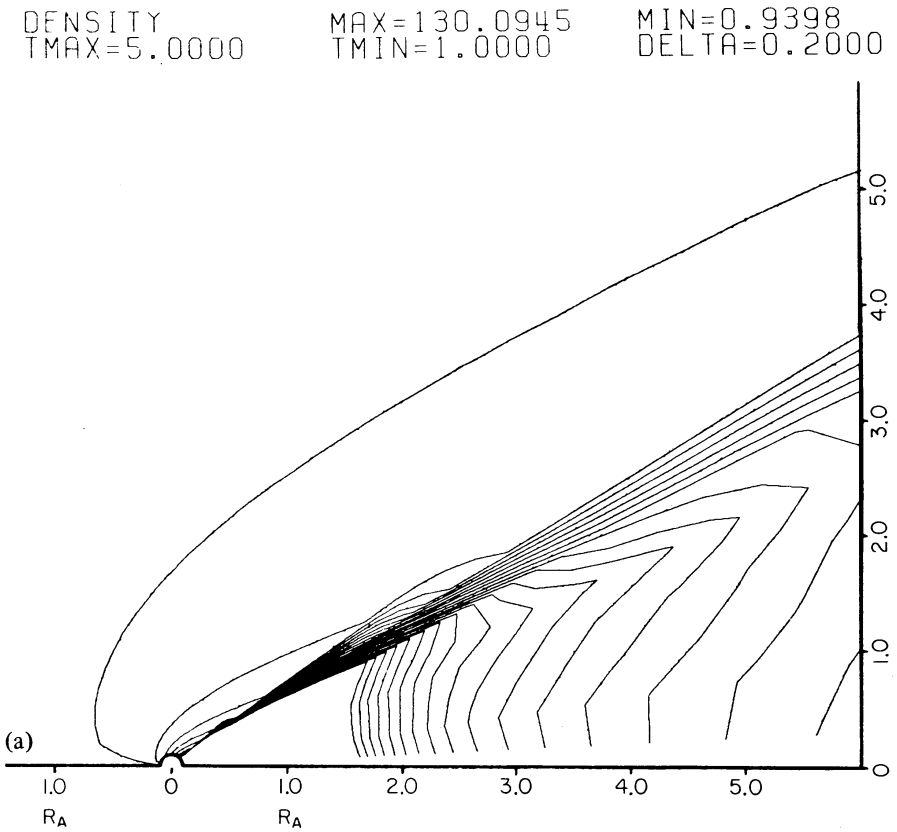

Figure 5. (a) Same as Fig. 4a except for specific heat ratio 1.1. (b) Same as Fig. 4b except for specific heat ratio 1.1. Gas accretes supersonically all over the spherical surface. (c) Same as Fig. 4c except for specific heat ratio 1.1.

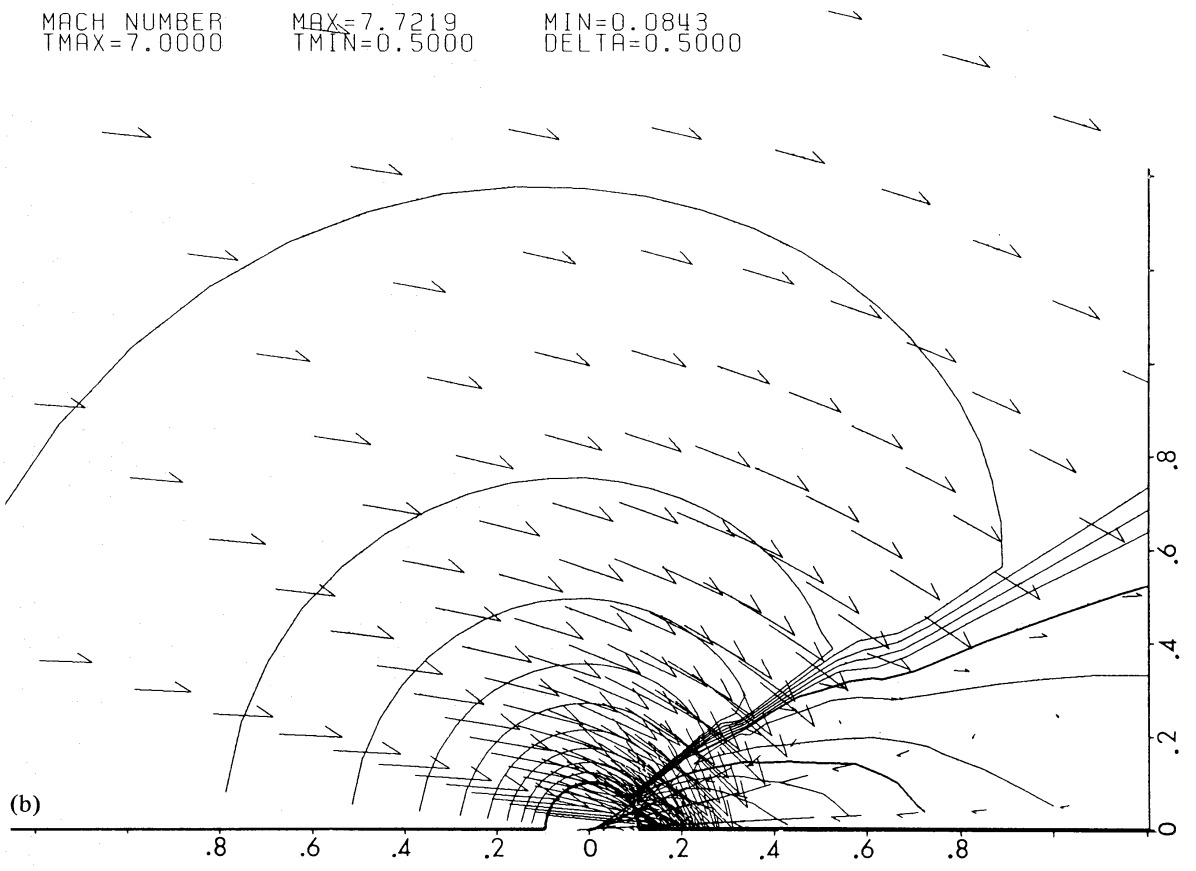

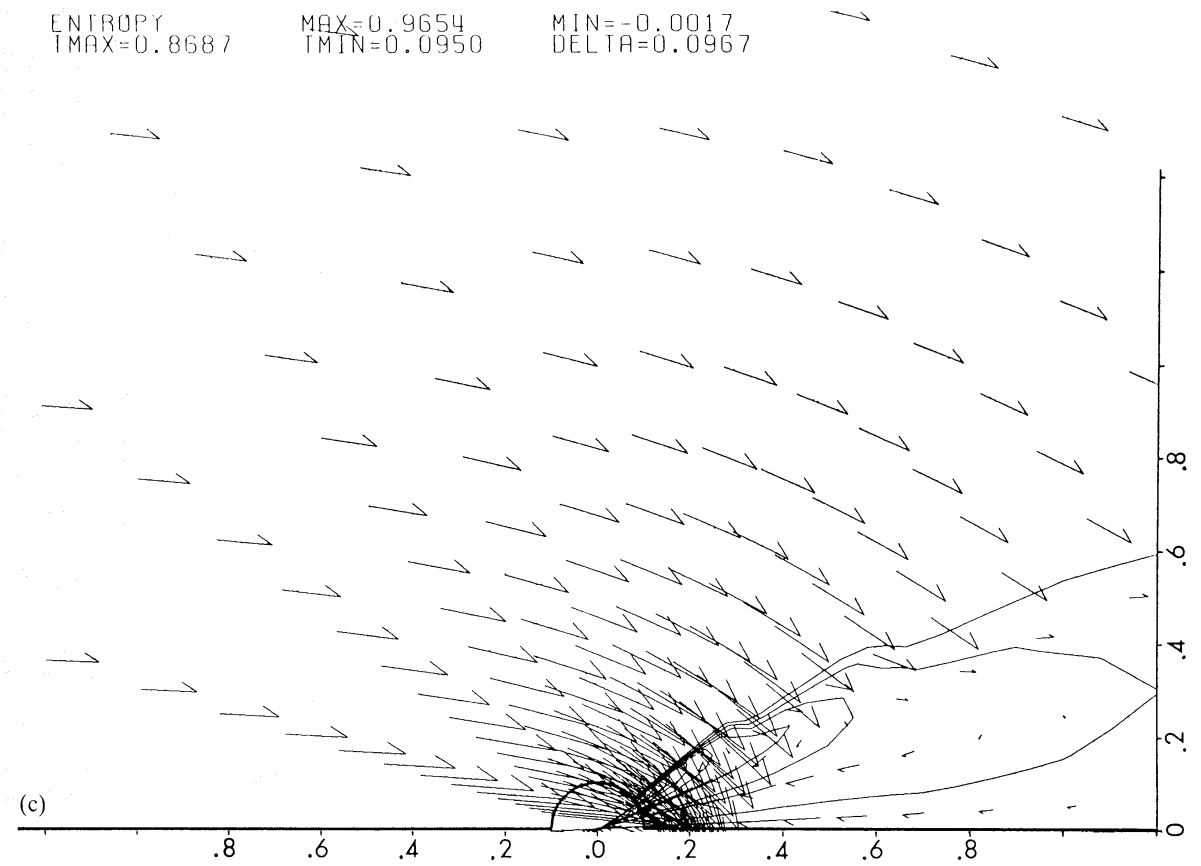

Figure 5 – *continued*

Fig. 4a, b and c show the density, the Mach number and the entropy contours in the case of $M_\infty=2.4$ and $\gamma=5/3$, while Fig. 5a, b and c illustrate those for $\gamma=1.1$. The position of shock wave and density distribution for $\gamma=1.1$ is quite different from those for the case of $\gamma=5/3$, which shows the bow shock wave. For smaller specific heat ratio, the shock angle becomes smaller and the shock location is shifted backward. The gas along the axis is as dense that as near the shock surface, and an 'accretion column' is formed. The maximum value of the density becomes larger for smaller specific heat ratio.

In the case of $\gamma=5/3$ the gas accretes subsonically, while in the case of $\gamma=4/3$ and 1.1 the material accreting from behind is accelerated to become supersonic. The Mach number of accreting flow is larger than unity all over the surface of the sphere in the latter two cases. At the shock surface, the direction of velocity is deflected sharply.

The flow with $\gamma=4/3$ was calculated by Hunt (1979), who showed that the primary shock was indented and that there existed a triple shock structure very close to the central body. In our calculations such features are not observed because the location of the triple shocks is at about $0.04R_A$ according to Hunt, which is inside our central hollow sphere. An indication of the indented shock is visible, though.

It should also be pointed out that we do not obtain flow patterns containing a hollow cone as suggested by Bisnovatyi-Kogan *et al.* (1979). There is no point of infinite density either on the axis or on a cone. Their solutions are obtained on the assumption of infinite R_A (infinite δ), while in our solutions $\delta=10$.

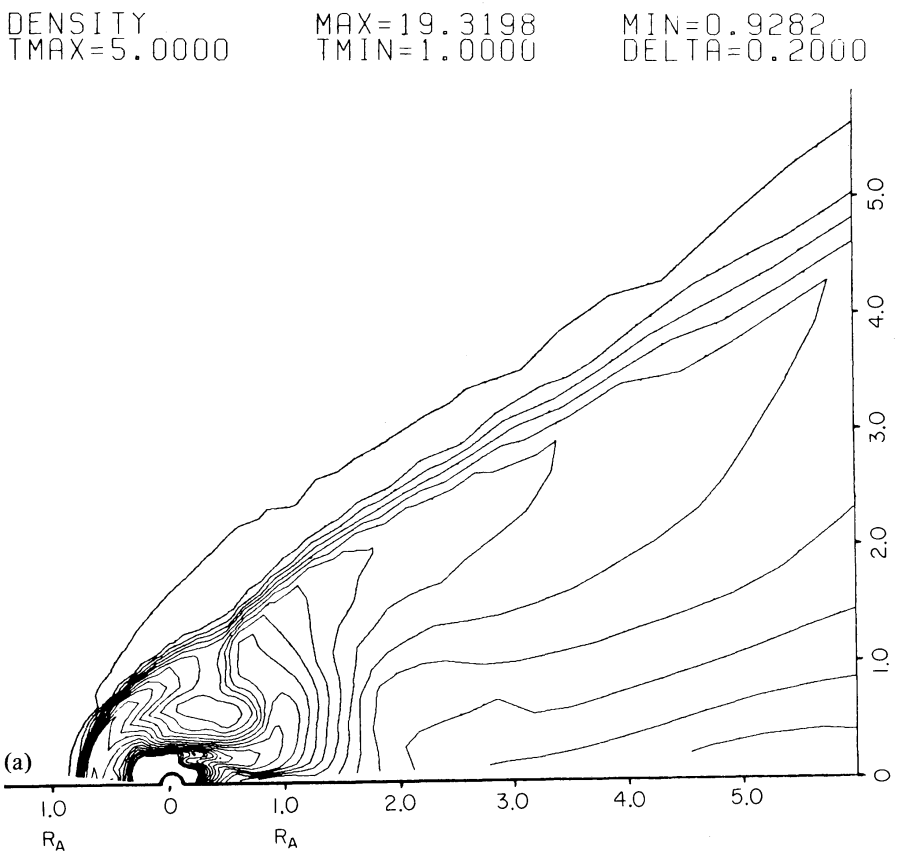

Figure 6. (a) The density contours for the flow about a gravitating rigid sphere. The Mach number is 2.4. The detached bow shock is observed. Compare this figure with Fig. 4a. The density patterns at the outer region are almost same for both figures. Therefore, the outer flow field is independent of the inner boundary condition. (b) The Mach number contours for the same model as Fig. 6a. Note that the complex counter currents (or vortex rings) are formed close to the body. (c) The entropy contours for the same model as Fig. 6a.

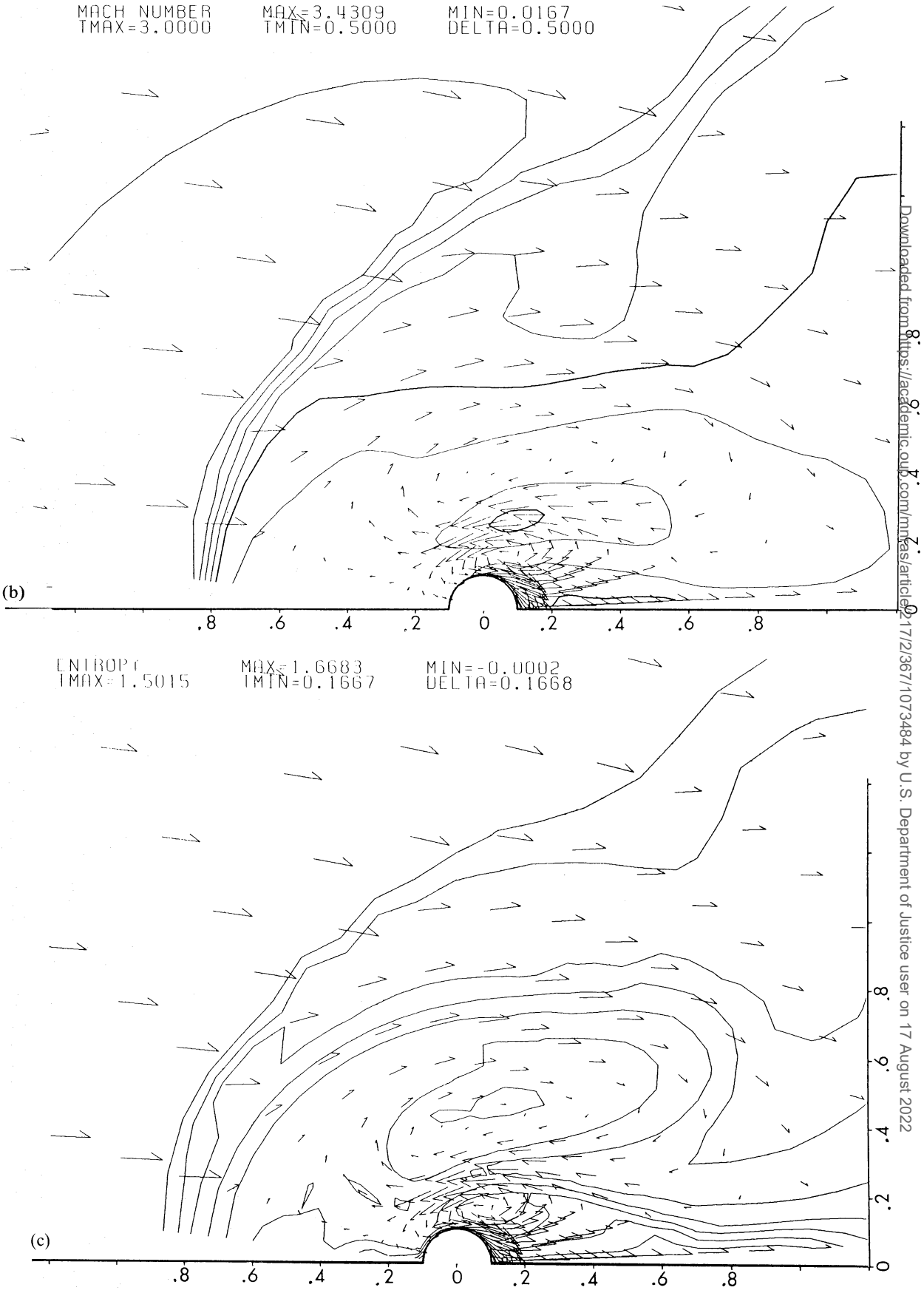

Figure 6 – *continued*

3.4 FLOW ABOUT A GRAVITATING RIGID SPHERE

For the subsonic case, a gas is attracted by the gravitational attraction due to the body and a dense atmosphere is formed near the body. The density distribution is almost isotropic about the body. The flow pattern is similar to that of non-gravitating subsonic cases.

In supersonic cases, a rather complex density distribution and velocity field are found. Fig. 6a, b and c show the density, the Mach number and the entropy contours for the Mach number of 2.4. Counter-current regions (or vortex rings) about the body can be seen. This phenomenon was also observed by Shara & Shaviv (1980) for hypersonic flows, and by Sakurai (1983) for subsonic Stokes flows, and Takeda *et al.* (1985) for supersonic viscous flows about a gravitating solid sphere. The size of the vortex ring given by Shara & Shaviv is much larger than that by other authors.

Vorticity can be induced either by a shock or numerical viscosity in an inviscid flow. It is very difficult to model such structures since the induced velocity depends on the numerical viscosity, which depends on the mesh Reynolds number. This, in a second-order code, is approximately (size of region/mesh spacing)^2, i.e. about 10^2 in our case. Therefore the precise structure of the inner flow may depend in the numerical resolution. Nevertheless we believe that such vortex rings exist in the flow about a gravitating rigid sphere because the computation of a flow about a non-gravitating rigid sphere does not show such structure.

Although the present flow does not approach steady state in a strict sense for supersonic cases, the flow can be considered to be in a quasi-steady state, since the basic flow pattern (number of vortex rings, etc.) does not change with time. Such oscillations are also observed by Takeda *et al.* (1985). The period of an oscillation includes more than 10^3 numerical time steps, and is of the order of (accretion radius/sound speed). This oscillation is probably due to a gravitational wave in the atmosphere formed about the body.

Comparing Fig. 6a with Fig. 4a, one can conclude that the general shape of the shock wave and the density distribution outside the accretion radius are similar to those in the accreting case. Our shock is conical except near the sphere, where a bow shock is observed. As was stated in the introduction, this result is very different from that of Shara & Shaviv (1980), which does not show any shock-like features. These authors try to identify the shock with the sonic line and conclude that the shock surrounds the body.

This identification is not valid, since supersonic-supersonic transitions can occur in an oblique shock as is shown in Fig. 3b. In reality the velocity component normal to the shock changes from supersonic to subsonic. Therefore they merely identify a part of the shock and a sonic line behind the body where subsonic to supersonic transition ocurs.

Shara & Shaviv state that the shock is round. However, it is hard to understand such a statement since a solid body cannot absorb gas. The shape of the shock should be open except during an initial transient phase. We actually observe a round shock in the initial transient stage of our calculations. Their results are probably due to the fact that either a (quasi) steady state is not reached or a shock transition is too much smeared out by the switched Shuman filter adopted by them.

3.5 COEFFICIENT OF DRAG

A moving sphere in a gas generally feels a drag. However a (gravitating) rigid sphere moving in an inviscid gas subsonically does not feel any drag, because the atmosphere formed around the body is spherically symmetric. If it moves supersonically, it generates waves and experiences a drag. An accreting body always feels a drag since the momentum of the absorbed gas is given to the body.

The drag can be computed by considering two contributions: the first is a drag due to aerodynamic force, which is computed by integrating the momentum flux all over the body surface; the second comes from the front–rear asymmetry of gravitational attraction from the atmosphere. Each drag coefficient is defined as

C_{dA}=(drag by aerodynamic force)/$\frac{1}{2}\pi R_{\mathrm{A}}^2 \varrho_\infty V^2$,

C_{dG}=(drag by gravitational force)/$\frac{1}{2}\pi R_{\mathrm{A}}^2 \varrho_\infty V^2$,

$C_{dT}=C_{dA}+C_{dG}$.

The present definition of the drag coefficient is different from the conventional one in which R_{A} is replaced with the radius of the body. In order to have the conventional definition, C_{dT} should be multiplied by δ^2.

Table 1 shows the drag coefficients for the accretion models. It is interesting to note that c_{dA} is

Table 1. Table of drag coefficients for accretion models. c_{dA} represents the aerodynamic contribution, c_{dG} the gravitational contribution and c_{dT} the total drag coefficient. The drag coefficient is normalized by the accretion radius R_{A}. The minus sign shows a thrust rather than a drag.

Mach No.	γ	c_{dA}	c_{dG}	c_{dT}
0.6	1.1	0.24	0.27	0.51
0.6	4/3	0.24	0.12	0.36
0.6	5/3	0.24	0.13	0.37
1.4	1.1	−3.34	9.22	5.88
1.4	4/3	−2.02	7.80	5.78
1.4	5/3	−0.04	4.57	4.53
2.4	1.1	−4.02	11.2	7.18
2.4	4/3	−2.70	9.57	6.87
2.4	5/3	−1.05	6.99	5.94
5.0	4/3	−2.93	9.81	6.88
5.0	5/3	−1.47	7.77	6.30

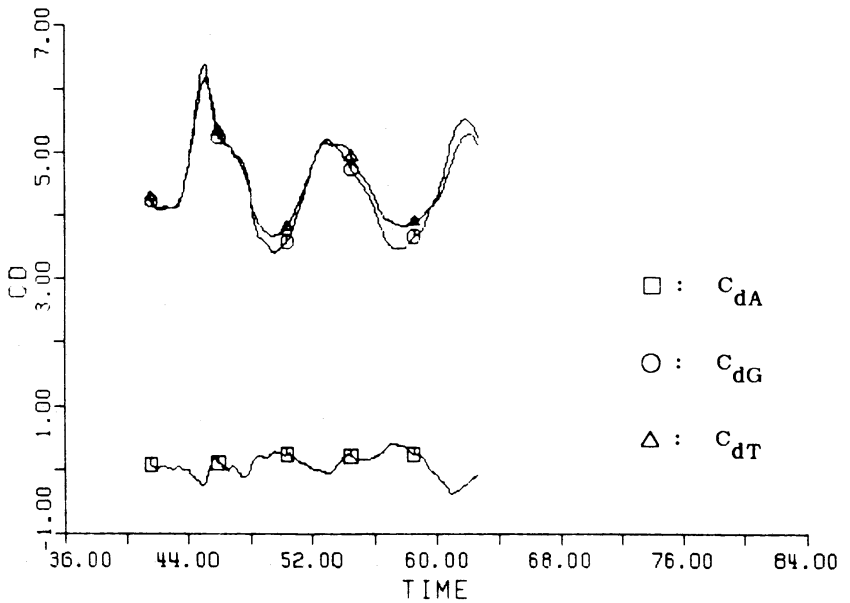

Figure 7. Time evolution of the drag coefficients for the flow about the gravitating rigid sphere. The Mach number is 5.0.

negative (i.e. a thrust) for supersonic flows. This is because a dense gas is mainly absorbed from the rear side of the body.

In the case of the solid sphere, c_{dA} is negligible compared with c_{dG}, and each contribution is not tabulated. The time evolution of the drag coefficient in the case of the solid sphere with Mach 5.0 is presented in Fig. 7. Because of the unsteady nature of the flow, the oscillation of the drag coefficient is found for the supersonic cases. The mean value of C_{dT} is about 5.

The coefficients of total drag for various models are summarized in Fig. 8, and is about 4–7, which is also consistent with the theoretical estimate, equation (3.2), to be discussed below. It

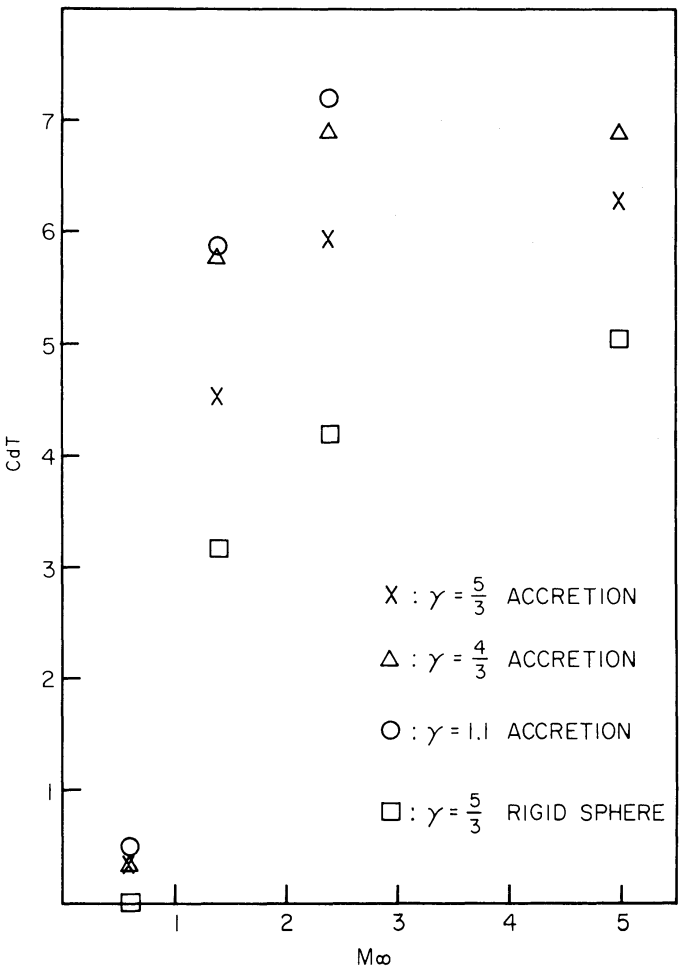

Figure 8. The coefficient of the total drag is plotted as a function of the Mach number and the specific heat ratio.

should be noted that the drag for the solid sphere moving subsonically is zero within an error.

We must admit that the calculation requires longer computation time for the lower specific heat ratio, and therefore the flow for γ=1.1 may not reach to a complete steady state.

The drag force F for the supersonic flow is estimated to be (Dokuchaev 1964; Ruderman & Spiegel 1971; Rephaeli & Salpeter 1980)

$$F \sim \pi R_A^2 \varrho V^2 \ln(b_{max}/b_{min}), \tag{3.1}$$

where b_{max} and b_{min} are the gravitational upper and lower cut-off distances, respectively. The drag coefficient in the present notation is therefore

$$C_d \sim 2 \ln(b_{max}/b_{min}). \tag{3.2}$$

We may identify b_{max} with r_{max}. If we take b_{min} to be r_{min}, then $b_{max}/b_{min}=116$, and we have $C_d=9.5$. Since equation (3.1) is based on a small perturbation theory, it may be appropriate to take b_{min} to be R_A. In this case we have $b_{max}/b_{min}=11.6$ and $c_d=4.9$. In any case these theoretical estimates are consistent with our numerical results.

Shara & Shaviv (1980) also computed C_d for the flow with the Mach number of 14.76 and $\delta=4$, and obtained $C_d\sim 1/8$ in our notation. Thus their drag coefficient is almost two orders of magnitude smaller than the above theoretical estimate.

3.6 ACCRETION RATE

Let us define the effective accretion radius R_{Ae} by

$$\pi R_{Ae}^2 \rho_\infty V = A, \tag{3.3}$$

where A is the accretion rate. In the 'line accretion theory' (Hoyle & Lyttleton 1939), the accretion rate A is given by equation (1.1), and R_{Ae}/R_A is unity.

In the 'column accretion theory' (Bondi & Hoyle 1944), the accretion rate is given by (1.2). The value of R_{Ae}/R_A is $\alpha^{1/2}$, which is 0.7–1. Bondi's interpolation formula equation (1.6) suggests that

$$R_{Ae}/R_A = 2^{-1/2}\{M_\infty^2/(M_\infty^2+1)\}^{3/4}. \tag{3.4}$$

Fig. 9 shows the values of R_{Ae}/R_A obtained by the numerical integration of the mass flux at the inner boundary. In Fig. 9 R_{Ae}/R_A predicted by Bondi's interpolation formula is shown by a continuous line, which does not agree with our results.

If we multiply the above formula by $2^{1/2}$, which is shown by the dash–dot line, then better

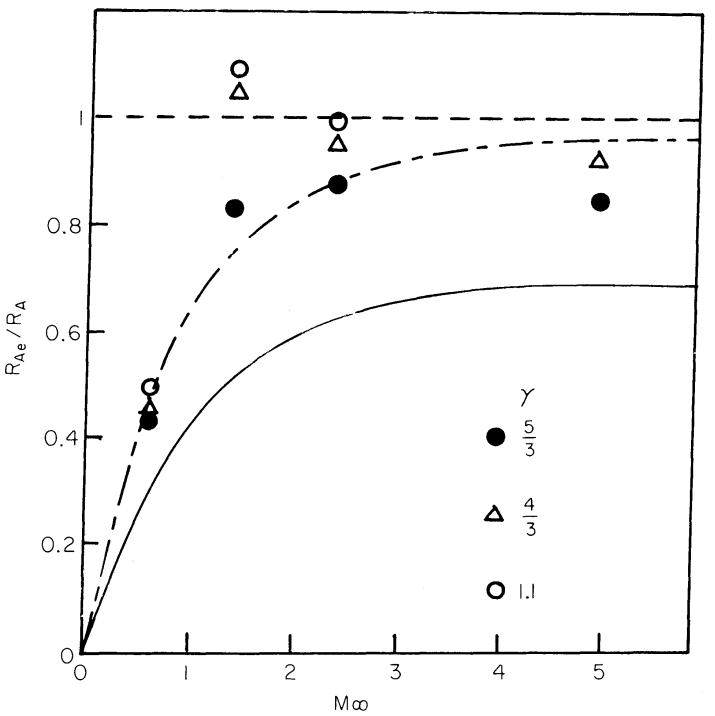

Figure 9. The effective accretion radius is shown as a function of the Mach number and the specific heat ratio. Bondi's interpolation formula is represented by the continuous line, while the dash–dot line shows our modified formula. The dotted line shows the limiting value due to Hoyle & Lyttleton.

agreement is achieved. The modification suggest that the Bondi's interpolation formula (1.6) should be doubled. This modification seems to be very reasonable, since it approaches equation (1.1) for large Mach number.

Hunt (1979) reported that the accretion rate is at least twice the value predicted by Hoyle & Lyttleton for higher Mach number and $\gamma=4/3$. Our $r_{\max}$ is about $10R_A$, while Hunt's is much larger. It may be argued that this fact explain the difference between two results. In order to take into account of this effect, the analytic solution based on the cold gas model (Bisnovatyi-Kogan *et al.* 1979) is used for the upstream boundary condition instead of the uniform flow. We find that the accretion rate increases only a few per cent. Therefore the difference in size of the outer boundary cannot account for the quantitative disagreement between our result and Hunt's.

The accretion rate is determined by the stagnation point on the axis, at which velocity of the gas becomes zero. The precise position of the stagnation point is sensitive to the structure of the inner flow. Since our grid is much finer than Hunt's in these regions, our inner flow is more accurate than his. Therefore we believe that our result is better. It is to be hoped to clarify the cause of this discrepancy.

Acknowledgments

The authors are grateful to Prof. T. Sakurai for his discussions. Numerical calculations were carried our on the Fujitsu VP-100 vector processor and the M382 scalar processor at the Data Processing Centre of Kyoto University and on the Fujitsu M-380 at the Institute of Space and Astronautics Science. This work was supported by the Grant-in-Aid for Scientific Research (59540155) of the Ministry of Education and Culture in Japan.

References

Bisnovatyi-Kogan, G. S., Kazhdan, Ya. M., Klypin, A. A., Lutskii, A. E. & Shakra, N. I., 1979. *Soviet Astr.*, **23,** 202.
Bondi, H., 1952. *Mon. Not. R. astr. Soc.*, **112,** 195.
Bondi, H. & Hoyle, F., 1944. *Mon. Not. R. astr. Soc.*, **104,** 273.
Chakravarthy, S. R. & Osher, S., 1983. *A.I.A.A.Jl,* **29,** 1241.
Dokuchaev, V. P., 1964. *Soviet. Astr.*, **8,** 23.
Godunov, S. K., 1959. *Math. Sbornik,* **47,** 271.
Hoyle, F. & Lyttleton, R. A., 1939. *Proc. Camb. Phil. Soc.*, **35,** 405.
Hunt, R., 1971. *Mon. Not. R. astr. Soc.*, **154,** 141.
Hunt, R., 1979. *Mon. Not. R. astr. Soc.*, **188,** 83.
Jameson, A. & Baker, T. J., 1983. *A.I.A.A., Paper 83-1929*, 293.
Lees, L., 1955. *Proc. 5th Int. Aero. Conf. Los Angeles Inst. Aero. Soc.*, New York, p. 241.
Livio, M., Shara, M. M. & Shaviv, G., 1979. *Astrophys. J.*, **233,** 704.
Osher, S. & Chakravarthy, S., 1983. *J. Comp. Phys.*, **50,** 447.
Rephaeli, Y. & Salpeter,. E. E., 1980. *Astrophys. J.*, **240,** 20.
Rizzi, A., 1982. *A.I.A.A.Jl,* **20,** 1329.
Ruderman, M. A. & Spiegel, E. A., 1971. *Astrophys. J.*, **165,** 1.
Sakurai, T., 1983. *Geophys. Astrophys. Fluid Dynamics,* **24,** 225.
Shara, M. M. & Shaviv, G., 1980. *Astrophys. Space Sci.*, **67,** 427.
Takeda, H., Matsuda, T., Sawada, K. & Hayashi, C., 1985. *Prog. Theor. Phys.*, **74,** 272.
van Albada, G. D., van Leer, B. & Roberts, W. W., 1982. *Astr. Astrophys.*, **43,** 76.
Van Dyke, M., 1982. *An Album of Fluid Motion*, The Parabolic Press.
Wolfson, R., 1977. *Astrophys. J.*, **213,** 200.